

EFFECT OF SUBSOIL CLAY LAYERS ON THE SEISMIC BEHAVIOUR OF EMBANKMENTS

Kyoto University Student Member ○Sadeghi Hamidreza
 Kyoto University Fellow Member Oka Fusao
 Kyoto University Member Kimoto Sayuri

1. INTRODUCTION

Road embankments are essential infrastructures of each country that are sometimes quite vulnerable to earthquake damages. Liquefaction-induced settlement and spreading caused by earthquake are major causes of damage to such structures. Based on loading conditions and formation of subsoil layers, numerous patterns of failure can be assumed for an embankment. Sasaki et al. (1994) reported various failure modes in dikes and road embankments. OKA et al. (2012) presented the main causes and patterns of river embankment damages during 2011 off the pacific coast of Tohoku earthquake. He mentioned the effects of subsoil clay profiles and duration time of earthquake motions. In this paper, the analysis results of an embankment on a layered ground consisting of clay and loose sand layers subjected to a long duration simulated earthquake are presented and the effects of clay layer's stiffness are discussed.

2. CONSTITUTIVE MODEL & MATERIALS

The constitutive model used for sandy layers is the Elasto-Plastic (EP) cyclic model for sands developed by Oka et al. (1999), while an elasto-viscoplastic (EVP) model by Kimoto et al. (2012) is employed for the clay. The elasto-viscoplastic model considers the structural degradation of the soil skeleton by the shrinkage of overconsolidation boundary surface and static yield surface regarding the accumulation of viscoplastic strain. Derivation is based on an overstress type of viscoplasticity theory and the non-associated flow rule. The nonlinear kinematic hardening rule is adapted into the viscoplastic strain dependency of shear modulus. The strain rate tensor consists of elastic and viscoplastic strain rates defined as:

$$\dot{\epsilon}_{ij} = \dot{\epsilon}_{ij}^e + \dot{\epsilon}_{ij}^{vp} \quad (1)$$

$$\dot{\epsilon}_{ij}^e = \frac{1}{2G} \dot{S}_{ij} + \frac{k}{3(1+e)} \frac{\dot{\sigma}'_m}{\sigma'_m} \delta_{ij}$$

Static yield function f_y is obtained by considering the nonlinear kinematic hardening rule for the changes in stress ratio, the mean effective stress, and viscoplastic volumetric strain (Sawada 2008) as:

$$f_y = \bar{\eta}_x^* + \tilde{M}^* \left\{ \ln \frac{\sigma'_{mk}}{\sigma'_{ms}} + \ln \left| \frac{\sigma'_m}{\sigma'_{mk}} - y_{m1}^* \right| \right\} \quad (2)$$

$$\bar{\eta}_x^* = \left((\eta_{ij}^* - \chi_{ij}^*) (\eta_{ij}^* - \chi_{ij}^*) \right)^{1/2}, \quad (3)$$

$$d\chi_{ij}^* = B^* (A^* d\epsilon_{ij}^{vp} - \chi_{ij}^* d\gamma^{vp}), \quad (4)$$

$$\gamma^{vp} = \int \left(\dot{\epsilon}_{kl}^{vp} \dot{\epsilon}_{kl}^{vp} \right)^{1/2} dt \quad (5)$$

where A^* and B^* are material parameters, $\dot{\epsilon}_v^{vp}$ is the viscoplastic deviatoric strain increment tensor, and γ^{vp} is the accumulated viscoplastic shear strain. The scalar kinematic hardening parameter y_{m1}^* is determined by

$$dy_{m1}^* = B^* \left(A^* d\epsilon_v^{vp} - y_{m1}^* \left| d\epsilon_v^{vp} \right| \right) \quad (6)$$

In this equation A_2^* and B_2^* are material parameters, and $\dot{\epsilon}_v^{vp}$ is the viscoplastic volumetric strain rate. The viscoplastic deviatoric strain rate and the viscoplastic volumetric one can be expressed as:

$$\dot{\epsilon}_{ij}^{vp} = C_1 \sigma'_m \exp \left\{ m' \left(\bar{\eta}_x^* + \tilde{M}^* \ln \frac{\sigma'_{mk}}{\sigma'_{mb}} + \ln \left| \frac{\sigma'_m}{\sigma'_{mk}} - y_{m1}^* \right| \right) \right\} \frac{\partial f_p}{\partial S_{ij}} \quad (7)$$

$$\dot{\epsilon}_v^{vp} = C_2 \sigma'_m \exp \left\{ m' \left(\bar{\eta}_x^* + \tilde{M}^* \ln \frac{\sigma'_{mk}}{\sigma'_{mb}} + \ln \left| \frac{\sigma'_m}{\sigma'_{mk}} - y_{m1}^* \right| \right) \right\} \frac{\partial f_p}{\partial \sigma'_m} \quad (8)$$

Refer to Oka et al. (1999) and Kimoto et al. (2012) for detail descriptions of the constitutive models. Table 1 shows the input data of the models.

Table 1 Material Properties

	Em (EP)	As-U (EP)	As-L (EP)	Dg1 (EP)	Ac (EVP)
Density ρ (t/m ³)	1.8, 2.0	1.8	1.8	1.9	1.66
Coefficient of Permeability K^*, γ_{v0} (m ⁴ /kN*s)	2.25×10^{-5}	3.89×10^{-8}	5.6×10^{-7}	1.0×10^{-6}	5.87×10^{-11}
Initial void ratio e_0	0.8	0.623	0.9	0.9	1.25
Compression index λ	0.025	0.0875	0.01	0.01	0.341
Swelling index κ	0.0003	0.0068	0.003	0.003	0.019
Initial elastic shear modulus ratio G_0/σ'_{m0}	761	175.5	512	541	75.2
Stress ratio at compression M'_{mc}	0.909	1.12	0.909	0.909	1.24
Stress ratio at failure M'_f	1.229	1.36	1.158	1.336	1.24
Hardening parameters B'_0, B'_1, C'_r	2000, 4, 0	3000, 5, 15	3800, 70, 0	3000, 5, 0	100, 40, 10
Structural parameters n, β	0.50, 50	-	-	-	0.30, 3.6
Dilatancy Parameters D'_0, n	1.0, 4.0	2.75, 4.75	1.00, 6.00	-	-
Reference value of plastic strain γ_r^{p*}	0.0050	0.0033	0.0050	-	-
Reference value of plastic strain γ_r^{e*}	0.003	0.019	0.010	-	-
Viscoplastic parameter m	-	-	-	-	24.68
Viscoplastic parameter C_1 (1/s)	-	-	-	-	$1.00 \times 10^{-5} / 10^{19}$
Viscoplastic parameter C_2 (1/s)	-	-	-	-	$3.83 \times 10^{-6} / 10^{20}$
Scalar hardening parameters A'_2, B'_2	-	-	-	-	5.9, 1.8
Strain-dependent parameters α, r	-	-	-	-	10, 0.4

3. ANALYSIS METHOD

Program COMVIDY-2D developed by Oka et al. (2013) was used in this simulation. This code adopts u - p formulation with the finite deformation FEM method. As for the discretization in the time domain, Newmark's β method is used. Rayleigh's damping is also applied, which is proportional to the initial stiffness and mass matrix.

4. FEM MODEL & BOUNDARY CONDITIONS

Fig.1 shows the finite element model of this analysis with 1140 eight-node plane strain elements. As for the boundary conditions, equal displacements have been applied to the right and left sides of the model. The nodes

Keywords: Liquefaction, Lateral Spreading, Failure Pattern, Strain Localization, Embankment
 615-8540, Kyoto University, Katsura Campus, C1-4, Geomechanics Lab, +81-75-383-3193

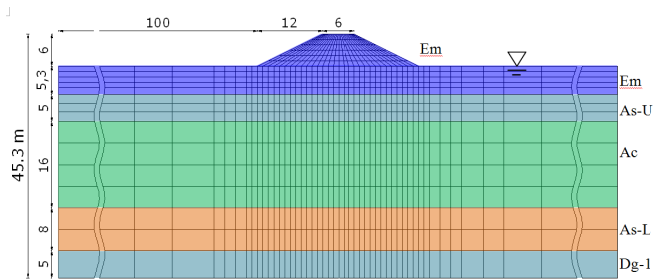


Fig. 1 FEM model of Torishima Embankment

of the bottom are also constrained in horizontal and vertical directions. Shown in Fig. 2, is the Kihanto input acceleration used in this study.

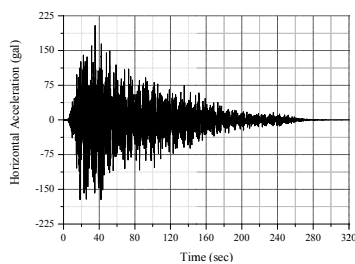


Fig. 2 simulated input acceleration (Kihanto)

5. RESULTS

As mentioned before, the effect of Ac clay layer's (Fig1.) stiffness has been controlled by parameters C_1 and C_2 as way the higher and lower values correspond to soft and stiff clay, respectively. Fig. 3 shows the deformed mesh of the two models. In all pictures a) stands for soft clay and b) corresponds to stiff clay case.

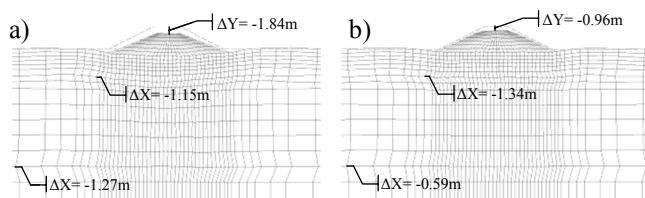


Fig. 3 Deformed mesh after 100 seconds

There is no need to emphasize on the point that the case with soft clay undergoes more settlement and lateral displacements. However, the interesting fact is that the large lateral displacements of the liquefied sandy layers in both cases continue to more than 40 meters away from the embankment's center. Fig. 4 shows the amount of effective stress decreasing ratio. Reviewing liquefied (ESDR=1.00) parts proves that liquefaction of the surface sand layers is the main cause of damage to both cases.

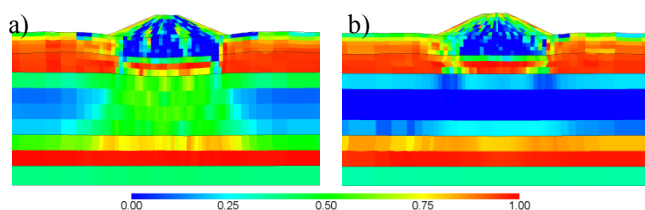


Fig. 4 ESDR after 60 seconds

Nevertheless, the failure modes seem to be quite different in the two. Although the As-U layer is completely liquefied in both cases, it is the stiffness of the clay layer that plays major roles in the deference of surface layer settlements. Fig. 5 shows the accumulated plastic deviatoric strains. It can be seen that the failure and strain localization patterns in soft clay resemble the punch failure of footing on highly compressible soils, while

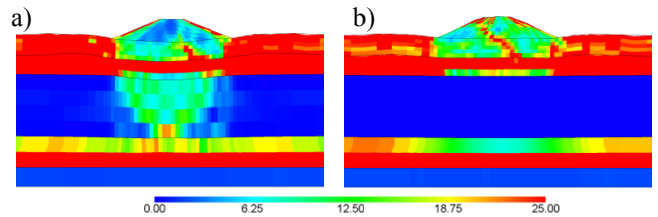


Fig. 5 Acc. plastic deviatoric strains (%) after 100 seconds

with the stiff clay, the embankment will experience deep sliding and inclined cracks.

6. CONCLUSIONS

Effects of clay layer's stiffness were studied using a large-deformation analysis program. The results agree with the failure patterns and sub-layer effects reported by Sasaki (1994) and Oka (2012). As expected, by assuming a stiffer clay layer, the amounts of settlements substantially reduce. Similarly, lateral deformations of the Ac clay layer reduce with the increasing of its stiffness, however, the stiffer the clay, the more spreading and lateral displacements of the surface layers and embankment. This proves that stiffer clay in the foundation will increase the lateral spreading of the embankment and reduce its settlements. In the stiff clay mode, localizations are seen in the body as inclined shear bands implying deep cracks in the field. But in soft clay mode, the shear bands and strain localizations distribute in the clay layer resembling a punch shear wedge. It must also be mentioned that attenuation caused by reductions in shear modulus of As-L layer during liquefaction, inhibited the propagation of the earthquake excitation to the upper layers, contributing to the reduction of damages to the embankment.

REFERENCES

- Kimoto, S., Shahbodagh Khan, B., Mirjalili, M., Oka, F.: Proc. 8th European Solid Mechanics Conf., Austria, 2012.
- Oka, F., Yashima, A., Tateishi, A., Taguchi, T., Yamashita, S.: J. Geotechnique, 49-5, pp.661-680, 1999.
- Oka, F., Tsai, P., Kimoto, S., Kato, R.: Soils & Foundations, 52-5, pp. 890-909, 2012.
- Oka, F., Shahbodaghkhan B., Kimoto, S., Sadeghi, H.: Program COMVIDY-2D, large deformation dynamic analysis based on the three-phase mixture theory, Geomechanics Lab, Kyoto University, Jan. 2013.
- Sawada, M.: Master thesis (in Japanese), Geomechanics Lab, Kyoto University, 2008.
- Sasaki, Y., Oshiki H., Nishikawa, J.: Proc., 13th ICSMFE, JGS, PP. 61-68, 1994.